Strongly confined, low-threshold laser modes in organic semiconductor microgoblets

Tobias Grossmann,[1,2,*] Sönke Klinkhammer,[3,2] Mario Hauser,[1] Dominik Floess,[1] Torsten Beck,[1] Christoph Vannahme,[2,3] Timo Mappes,[2] Uli Lemmer,[3] and Heinz Kalt[1]

[1]*Institute of Applied Physics, Karlsruhe Institute of Technology, 76128 Karlsruhe, Germany*
[2]*Institute of Microstructure Technology, Karlsruhe Institute of Technology, 76128 Karlsruhe, Germany*
[3]*Light Technology Institute, Karlsruhe Institute of Technology, 76128 Karlsruhe, Germany*
*tobias.grossmann@kit.edu

Abstract: We investigate lasing from high-Q, polymeric goblet-type microcavities covered by an organic semiconductor gain layer. We analyze the optical modes in the high-Q cavities using finite element simulations and present a numerical method to determine the cutoff thickness of the gain layer above which the whispering gallery modes are strongly confined in this layer. Fabricated devices show reduced lasing thresholds for increasing gain layer thicknesses, which can be explained by a higher filling factor of the optical modes in the gain layer. Furthermore, reduced lasing threshold is accompanied by a red-shift of the laser emission.

©2011 Optical Society of America

OCIS codes: (140.3948) Microcavity devices; (140.7300) Visible lasers; (160.4890) Organic materials; (160.5470) Polymers.

References and links

1. H.-S. Hsu, C. Cai, and A. M. Armani, "Ultra-low-threshold Er:Yb sol-gel microlaser on silicon," Opt. Express **17**(25), 23265–23271 (2009).
2. J. Yang and L. J. Guo, "Optical sensors based on active microcavities," IEEE J. Quantum Electron. **12**(1), 143–147 (2006).
3. E. P. Ostby and K. J. Vahala, "Yb-doped glass microcavity laser operation in water," Opt. Lett. **34**(8), 1153–1155 (2009).
4. W. Fang, D. B. Buchholz, R. C. Bailey, J. T. Hupp, R. P. H. Chang, and H. Cao, "Detection of chemical species using ultraviolet microdisk lasers," Appl. Phys. Lett. **85**(17), 3666–3668 (2004).
5. H. Rong, S. Xu, Y.-H. Kuo, V. Sih, O. Cohen, O. Raday, and M. Paniccia, "Low-threshold continuous-wave Raman silicon laser," Nat. Photonics **1**(4), 232–237 (2007).
6. P. Thilakan, G. Sasikala, and I. Suemune, "Fabrication and characterization of a high Q microdisc laser using InAs quantum dot active regions," Nanotechnology **18**(5), 055401 (2007).
7. T. Grossmann, M. Hauser, T. Beck, C. Gohn-Kreuz, M. Karl, H. Kalt, C. Vannahme, and T. Mappes, "High-q conical polymeric microcavities," Appl. Phys. Lett. **96**(1), 013303 (2010).
8. A. M. Armani, A. Srinivasan, and K. J. Vahala, "Soft lithographic fabrication of high Q polymer microcavity arrays," Nano Lett. **7**(6), 1823–1826 (2007).
9. S. Klinkhammer, T. Grossmann, K. Lull, M. Hauser, C. Vannahme, T. Mappes, H. Kalt, and U. Lemmer, "Diode-pumped organic semiconductor microcone laser," IEEE Photon. Technol. Lett. **23**(8), 489–491 (2011).
10. L. Yang, T. Carmon, B. Min, S. M. Spillane, and K. J. Vahala, "Erbium-doped and Raman microlasers on a silicon chip fabricated by the sol-gel process," Appl. Phys. Lett. **86**(9), 091114 (2005).
11. T. Grossmann, S. Schleede, M. Hauser, M. B. Christiansen, C. Vannahme, C. Eschenbaum, S. Klinkhammer, T. Beck, J. Fuchs, G. U. Nienhaus, U. Lemmer, A. Kristensen, T. Mappes, and H. Kalt, "Low-threshold conical microcavity dye lasers," Appl. Phys. Lett. **97**(6), 063304 (2010).
12. B. Min, S. Kim, K. Okamoto, L. Yang, A. Scherer, H. Atwater, and K. Vahala, "Ultralow threshold on-chip microcavity nanocrystal quantum dot lasers," Appl. Phys. Lett. **89**(19), 191124 (2006).
13. A. Tulek, D. Akbulut, and M. Bayindir, "Ultralow threshold laser action from toroidal polymer microcavity," Appl. Phys. Lett. **94**(20), 203302 (2009).
14. H. S. Choi, X. Zhang, and A. M. Armani, "Hybrid silica-polymer ultra-high-*Q* microresonators," Opt. Lett. **35**(4), 459–461 (2010).
15. G.-D. Kim, G.-S. Son, H.-S. Lee, K.-D. Kim, and S.-S. Lee, "Refractometric sensor utilizing a vertically coupled polymeric microdisk resonator incorporating a high refractive index overlay," Opt. Lett. **34**(7), 1048–1050 (2009).

16. Y. Takezawa, N. Taketani, S. Tanno, and S. Ohara, "Empirical estimation method of intrinsic loss spectra in transparent amorphous polymers for plastic optical fibers," J. Appl. Polym. Sci. **46**(10), 1835–1841 (1992).
17. J. Pomplun, S. Burger, L. Zschiedrich, and F. Schmidt, "Adaptive finite element method for simulation of optical nano structures," Phys. Status Solidi B **244**(10), 3419–3434 (2007).
18. M. Oxborrow, "Traceable 2-D finite-element simulation of the whispering-gallery modes of axisymmetric electromagnetic resonators," IEEE Trans. Microw. Theory Tech. **55**(6), 1209–1218 (2007).
19. T. A. Beierlein, B. Ruhstaller, D. J. Gundlach, H. Riel, S. Karg, C. Rost, and W. Rieß, "Investigation of internal processes in organic light-emitting devices using thin sensing layers," Synth. Met. **138**(1-2), 213–221 (2003).
20. M. M. Mazumder, G. Chen, R. K. Chang, and J. B. Gillespie, "Wavelength shifts of dye lasing in microdroplets: effect of absorption change," Opt. Lett. **20**(8), 878–880 (1995).

1. Introduction

Whispering gallery mode (WGM) microcavities with high quality factors (Q factors) are promising candidates for realizing low-threshold lasers that can be integrated on chip, and have great potential for applications in sensing [1–4] and telecommunications [5,6]. Besides high optical transparency, polymers are favorable for laser device fabrication due to large scale (soft-)lithographic structuring techniques, low material costs and simple doping with a broad variety of gain media. Currently, by either direct lithographic fabrication and subsequent surface tension-enhanced thermal reflow [7] or replica molding of an ultra-high-Q master [8], Q factors above 10^6 have been achieved in planar (on-chip), polymeric WGM-microresonators.

Besides a low-loss microresonator, a large oscillator strength gain medium has to be integrated in the device in order to achieve low lasing thresholds. The latter is desirable for utilization of compact pumping sources [9], ideally even incoherent light sources, such as light-emitting diodes. For this, gain materials can be directly integrated to the microcavity's material prior to the lithographic structuring. This is realized, e.g., in sol-gels doped with rare-earth ions [1,10] or in polymers doped with dye molecules [11]. Alternatively, a gain medium can be deposited onto the cavity subsequent to the lithographic structuring, e.g., by spin-coating [12–14] or sputtering [15].

In this work, we utilize the high refractive index organic semiconductor material tris(8-hydroxyquinoline) aluminum (Alq_3) doped with the laser dye 4-dicyanmethylene-2-methyl-6-(*p*-dimethylaminostyryl)-4H-pyran (DCM) on top of high-Q WGM-microcavities. In order to realize low-threshold lasing we adjust the gain layer thickness. By choosing the film thickness of the gain medium above a certain cutoff-thickness, the WGMs are almost completely localized in the gain layer leading to a significantly higher modal gain and strongly reduced mode volumes. We present a numerical method to determine the cutoff-thickness using finite element simulations and investigate the lasing behavior for three different gain-layer thicknesses in the different regimes identified by the numerical analysis, followed by a validation of the calculations by characterization of the fabricated devices.

2. High-Q microgoblet cavities

In the following, the manufacturing and the optical properties of the passive cavities are described before we turn to the analysis of the lasing properties.

In order to achieve low laser thresholds after deposition of the active layer, the Q factor of the WGM-microcavity has to be high. The cavities onto which the gain layer is deposited are goblet-shaped polymeric microcavities, which are made of the low-loss, thermoplastic polymer poly(methyl methacrylate) (PMMA) and are directly processed on a silicon substrate, see [7] for a detailed description. After lithographic structuring of PMMA-microdisks, the silicon is isotropically etched using XeF_2. A subsequent thermal reflow step results in goblet-shaped microcavities depicted in the scanning electron micrograph Fig. 1(a). These microcavities have a significantly reduced surface roughness compared to the microdisks before thermal treatment, resulting in a Q-factor enhancement by two orders of magnitude.

For measuring the quality factors of the WGMs in the microgoblets, a single-mode, tunable, external-cavity laser (linewidth 200 kHz) with wavelengths around 1300 nm is used.

Tapered optical fibers (SMF-28) with minimum waist diameters of approximately 1 µm are utilized to evanescently excite WGMs of the cavity. For resonator-waveguide positioning, the tapered fiber is mounted on a five axis positioning stage with a resolution of 20 nm. The transmitted intensity is recorded by a photodiode. The Q factors are determined by measuring the linewidth (full width at half maximum) of the Lorentzian-shaped dips in the transmission spectrum, recorded by sweeping the laser wavelength.
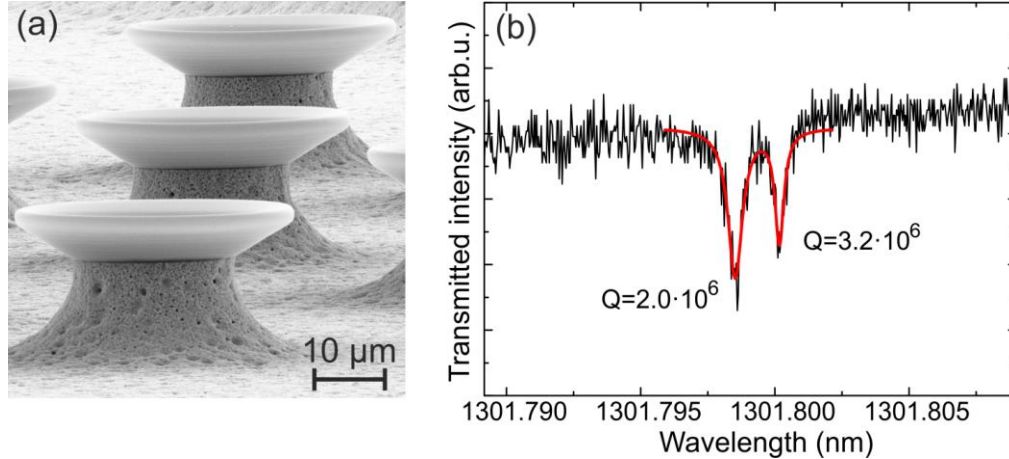

Fig. 1. (a) Scanning electron micrograph of an array of passive PMMA-microgoblets standing on silicon pedestals. (b) Transmission spectrum showing WGM-resonances with loaded Q factors of $3.2 \cdot 10^6$ and $2.0 \cdot 10^6$ inferred from the resonance linewidth, which is determined by a Lorenzian fit.

Figure 1(b) shows a resonance spectrum around 1301 nm of a goblet microcavity with a maximum diameter of 40 µm. The highest measured Q factor here is $3.2 \cdot 10^6$, indicating a smooth cavity surface with low surface-scattering losses of the WGMs. The Q factors in this wavelength region are mainly limited by the absorption of PMMA and are expected to be even higher in the visible [7,16].

3. Finite element simulations

In order to analyze the influence of an additional organic semiconductor coating with higher refractive index ($n_{Alq3:DCM} = 1.72$) than the PMMA-cavity ($n_{PMMA} = 1.49$) on the optical modes, we perform finite element simulations with JCMwave's simulation software package JCMsuite. We calculate the eigenvalues (frequencies) and the respective electric field distributions of the WGMs by solving Maxwell's equations with the eigensolver JCMresonance, using third order finite elements with adaptive mesh refinement [17]. In order to realize transparent boundary conditions, the simulation uses the adaptive perfectly matched layers method (PML).

Figure 2(a) shows the computational domain for modeling of microgoblet-lasers, where the rotational symmetry of the resonator is used to reduce computational costs. The inset of Fig. 2(a) shows an enlarged view of the resonator rim including the Alq$_3$:DCM-layer and the triangulation of the structure. The Alq$_3$:DCM-layer covers the upper half of the microresonator due to deposition of gain material from above by thermal evaporation. Each mode is characterized by the polarization of its electromagnetic field (tranverse electric (TE) or transverse magnetic (TM)), the azimuthal mode number m (integer number of wavelengths in the plane of the cavity), the axial mode number l and the radial mode number n. The modes in the following will be denoted as TE/TM$_{n,l}(m)$.

Figure 2(b) illustrates the effect of the Alq$_3$:DCM-layer on the WGMs for three different gain layer thicknesses d of 40, 80 and 200 nm, which were fabricated and characterized. For a

thickness of d = 40 nm the depicted intensity distribution of the fundamental $TM_{0,0}(274)$-mode sparsely overlaps with the gain layer. The same WGM in a cavity with a 80 nm thick Alq_3:DCM-layer is located closer to the cavity surface, thus having a larger overlap with the active material. For a gain layer thickness of 200 nm, the mode is guided in the high index material, resulting in a significantly larger confinement factor of the mode in the gain layer, which is advantageous for reducing the lasing threshold due to a high modal gain.
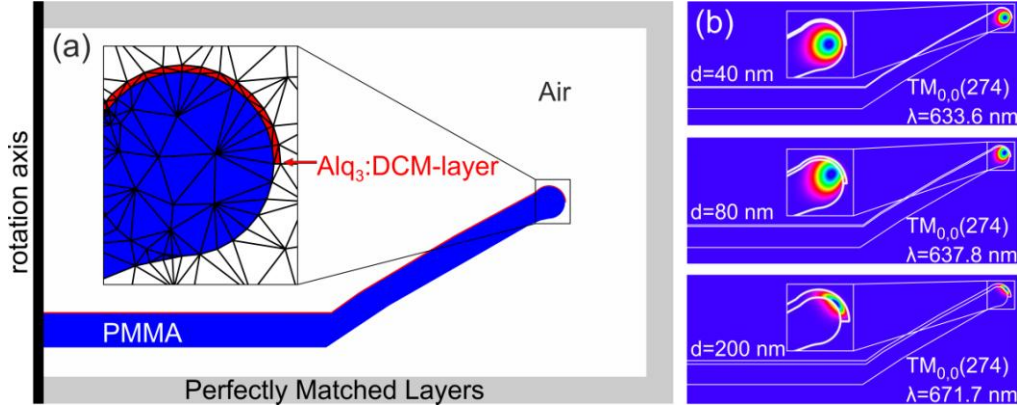
Fig. 2. (a) Computational domain for the finite element simulations showing the modeled cavity geometry and materials. The inset shows an enlarged view of the cavity rim with the gain material Alq_3:DCM on top of the PMMA-resonator and the initial triangulation for the computation. (b) Intensity distribution and resonance wavelengths of the $TM_{0,0}(274)$-mode for three different thicknesses of the Alq_3:DCM-layer. For a thickness of d = 200 nm of the Alq_3:DCM-layer, the mode is guided within the gain layer.

In order to derive a quantitative method for determining the cutoff-thickness, above which the mode is guided in the gain-layer, the effect of an increasing gain-layer thickness on the resonance wavelengths, the mode volumes and the filling factors of the WGMs were investigated in finite element simulations, in which the gain-layer thickness is varied between 5 and 300 nm in steps of 5 nm. As already noted in Fig. 2(b), the resonance wavelength of the same WGM increases with increasing thickness of the Alq_3:DCM-layer, as the mode is shifted to the gain layer and thus propagates along a slightly larger radius with a higher effective refractive index. This property is depicted in more detail in Fig. 3(a). Above a thickness of approximately 75 nm the splitting between TE and TM polarization increases, which also indicates a movement of the WGM intensity distribution towards the cavity surface, as shown in Fig. 2(b). Besides the effect of an increasing resonance wavelength, a change in the mode volume with increasing thickness of the gain layer can be observed in Fig. 2(b). Therefore the mode volume was calculated according to the following equation, where the dielectric constant is denoted as ε [18]:

$$V = \frac{\int \varepsilon \, |\vec{E}(r)|^2 \, dV}{\max\{\varepsilon \, |\vec{E}(r)|^2\}}.$$
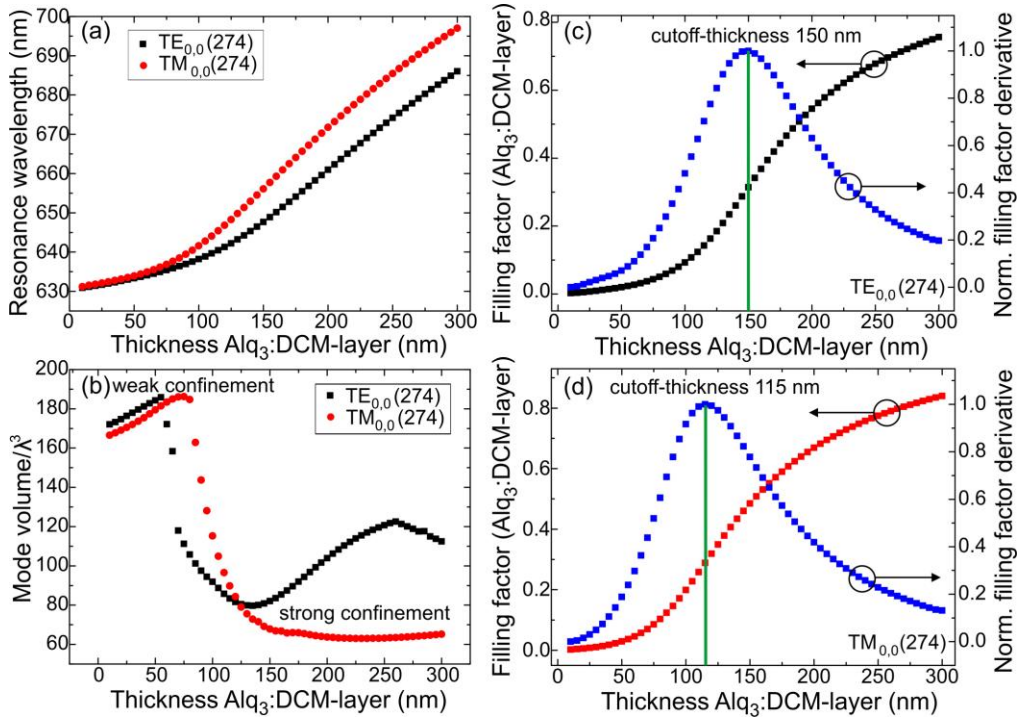
(1)

Fig. 3. Results of finite element calculations showing (a) the resonance wavelengths, (b) the mode volumes and the filling factors of the (c) $TE_{0,0}(274)$- and (d) $TM_{0,0}(274)$-modes as function of the Alq_3:DCM-layer thickness.

Figure 3(b) shows the mode volume as function of the Alq_3:DCM-layer thickness for the $TM/TE_{0,0}(274)$-mode. For both modes, the mode volume drops above a certain gain-layer thickness, due to the localization in the Alq_3:DCM. This enables identification of a weak and a strong confinement regime, indicated in Fig. 3(b). For the $TM_{0,0}(274)$-mode, the mode volume drops by a factor of three through the transition from weak to strong confinement.

Although a change in resonance wavelength and mode volume of the WGMs for larger thicknesses indicates guidance of the modes in the gain layer, a quantitative cut-off criterion cannot be inferred from these quantities. For this, we investigate the filling factor of the mode in the gain layer, defined as fraction of the electric energy density in the gain layer and the total electric energy density [18]:

$$F_g = \frac{\int_g \varepsilon \, |\vec{E}(r)|^2 \, dV}{\int \varepsilon \, |\vec{E}(r)|^2 \, dV}. \tag{2}$$

In this case, the filling factor F_g is a direct measure of the modal gain. The filling factor as function of the Alq_3:DCM-layer thickness for the fundamental TE- and TM-mode is depicted in Fig. 3(c) and Fig. 3(d), respectively. For both polarizations, the value of F_g is below 0.1 for gain-layer thicknesses under 100 nm. Above 100 nm, the filling factor strongly increases until saturation occurs for thicknesses above around 200 nm at values of $F_g \approx 0.8$. The strongest change in the filling factor occurs in the region where the mode changes its localization from the PMMA-layer to the Alq_3:DCM-layer. To visualize this, the derivative of the filling factor with respect to the thickness of the Alq_3:DCM-layer is depicted in Fig. 3(c) and Fig. 3(d). The derivative of the filling factor has a maximum at a certain thickness, which can be identified as cutoff-thickness. Below and above this thickness the change in F_g drops as the mode is either guided in the PMMA- or in the Alq_3:DCM-layer. The cutoff-thickness takes on values

of 115 and 150 nm for the analyzed fundamental TM- and TE-modes which feature resonance wavelengths within the spectral gain region of Alq_3:DCM.

4. Lasing in organic semiconductor coated microgoblets

In order to experimentally investigate the simulated effects of the identified regimes of low and high modal gain on the lasing threshold, samples with gain-layer thicknesses of 40 (weak mode confinement below cutoff), 80 (transition region) and 200 nm (strong mode confinement above cutoff) were fabricated. Thermal coevaporation of the organic semiconductor Alq_3 and the laser dye DCM (2.5 wt. %) on top of the microresonators was performed in a high vacuum evaporation chamber at a pressure of 10^{-6} mbar. Afterwards, the samples were encapsulated in a quartz cuvette under nitrogen atmosphere in order to prevent photooxidation of the active material under optical excitation.

The microcavities were optically pumped from above using a frequency-tripled Nd:YLF (neodymium-doped yttrium lithium fluoride) laser with pulse lengths < 5 ns at 349 nm. The emitted whispering-gallery laser light is collected in the plane of the microcavity by a multi-mode optical fiber connected to a spectrograph (Acton Research SpectraPro 300i) with CCD-camera.
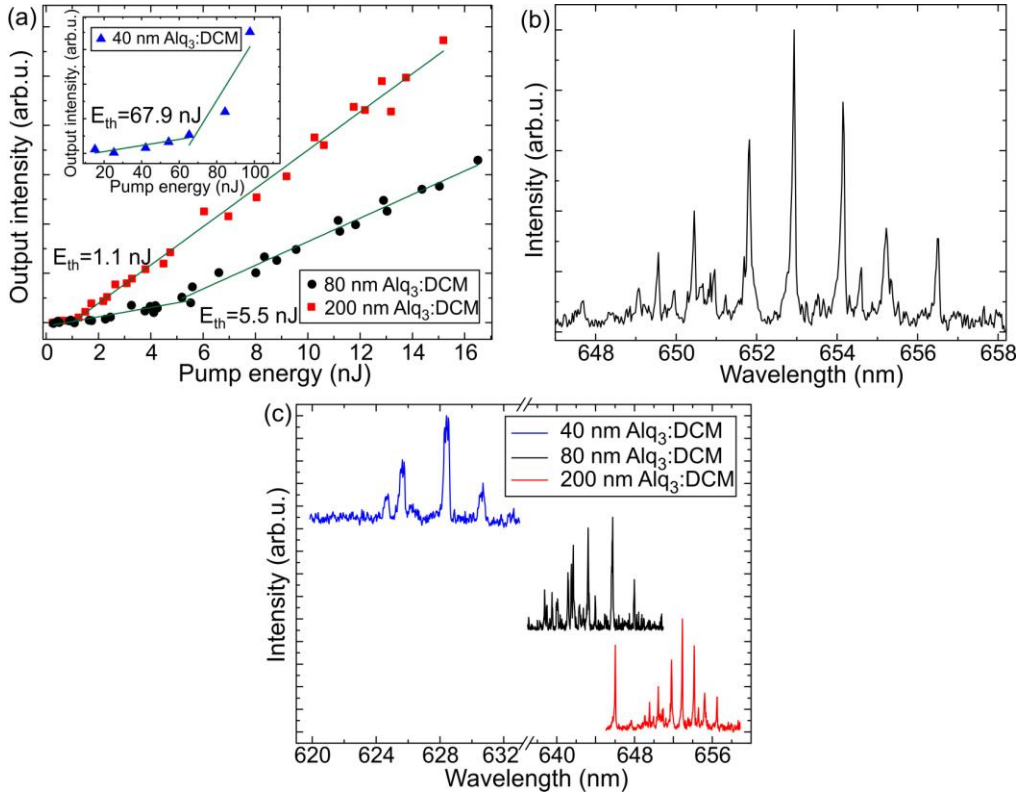

Fig. 4. (a) Input-output curves of microgoblet lasers with lasing thresholds of 67.9, 5.5 and 1.1 nJ covered with 40, 80 and 200 nm Alq_3:DCM, respectively. (b) Multi-mode lasing spectrum above threshold of the sample with 200 nm Alq_3:DCM with laser linewidths of 80 pm. (c) Comparison of the laser emission above threshold for the three Alq_3:DCM-layer thicknesses shows a red-shifted gain spectrum for thicker gain layers.

The input-output curves of optically pumped PMMA-microgoblets covered with a 40, 80 and 200 nm thick Alq_3:DCM-layer are shown in Fig. 4(a), where the lasing threshold energies E_{th} are determined by the onset of a superlinear output. For every excitation pump energy a

spectrum was acquired and integrated over the dominant laser line to obtain the output intensity. For the sample with 200 nm of Alq_3:DCM on top of the microcavities, the lasing-threshold energy was found to be as low as 1.1 nJ per pulse. As this gain-layer thickness is above cutoff, the lasing modes are guided in the high index material, resulting in a large filling factor of the modes in the gain layer. Based on typical values for the absorption of Alq_3 [19], the 200 nm thick gain layer is assumed to be nearly homogeneously pumped, so that many emitted photons experience amplification. This leads to a high modal gain and a reduced lasing threshold. For comparison with the regime below cutoff, two further Alq_3:DCM-thicknesses (40 and 80 nm) were characterized. For a thickness of 80 nm, the lasing threshold (E_{th} = 5.5 nJ) increases by a factor of 5 compared to the threshold above cutoff and even increases to a value of approximately 67.9 nJ (factor of more than 60 compared to the sample with 200 nm Alq_3:DCM) for an Alq_3:DCM-layer of 40 nm.

Besides the effect of higher modal gain, increasing filling factors of the modes in the Alq_3:DCM-layer lead to enhanced scattering of the WGMs at the DCM molecules and the inhomogeneities of the active medium. The low losses of the pristine cavity with Q factors above 10^6 are assumed to be negligible compared to the loss mechanisms caused by the active layer. Therefore, the Q factors of the Alq_3:DCM-covered microcavities are assumed to be reduced for increasing gain-layer thicknesses due to increased surface-scattering losses. Nevertheless, the measured lasing thresholds decrease with increasing gain-layer thickness indicating an overcompensation of a decreased Q factor by a strongly increased modal gain.

In addition to the optical losses, the microcavity determines the laser emission spectrum. Figure 4(b) shows a spectrum above threshold obtained from a microgoblet laser with a 200 nm thick Alq_3:DCM-layer. The multi-mode emission spectrum shows laser modes with linewidths of 80 pm, limited by the resolution of the spectrometer (1800 lines/mm grating). The wavelength spacing between observed lasing modes is smaller than the calculated free spectral range of about 2 nm due to the presence of higher-order transverse modes in addition to the fundamental cavity modes. Furthermore, the envelope of the laser emission is shifted to larger wavelengths for increasing Alq_3:DCM-layer thicknesses, shown in Fig. 4(c). This behavior is attributed to increased absorption of dye molecules for thicker gain layers due to an increased filling factor of the modes in the gain layer and results in red-shifted net gain spectra of the laser dye. This is accompanied by a decrease of the lasing thresholds due to an increased concentration of dye molecules within the WGMs. These effects can be described by a modified standard dye laser model [11,20], where the number of dye molecules per mode volume depends on the thickness of the gain layer.

5. Conclusion

In summary, we have numerically analyzed and subsequently fabricated and characterized PMMA-microgoblets covered with the organic semiconductor Alq_3:DCM with strongly confined, low-threshold laser modes. Owing to the higher refractive index of the Alq_3:DCM-layer compared to the underlying PMMA-microcavity, the WGMs are guided in the active layer above a certain cutoff thickness, which can be quantitatively determined by analyzing the filling factor of the modes in the gain layer using finite element simulations. Due to the large filling factors of the modes in this layer, the modes experience a higher modal gain and are confined to smaller volumes compared to Alq_3:DCM-layer thicknesses below cutoff. The demonstrated low lasing threshold of 1.1 nJ in the strongly confined regime is significantly lower than compared to the fabricated lasers with Alq_3:DCM-layer thicknesses below cutoff. The decreased lasing thresholds observed for thicker Alq_3:DCM-layers come along with red-shifted emission spectra, typical for dye lasers. The low threshold of microgoblet laser modes in the strongly confined regime allow for optical pumping using a low-cost, compact blu-ray laserdiode [9], which could pave the way towards development of ultra-compact photonic devices utilizing low-cost, polymeric, WGM-microcavity lasers.

Acknowledgments